THE JOURNAL OF PHYSICAL CHEMISTRY B

Article

pubs.acs.org/JPCB

Sensing Conformational Changes in DNA upon Ligand Binding Using QCM-D. Polyamine Condensation and Rad51 Extension of DNA Layers

Lu Sun,[†] Karolin Frykholm,[†] Louise H. Fornander,[†] Sofia Svedhem,[‡] Fredrik Westerlund,[†] and Björn Åkerman*[,†]

[†]Department of Chemical and Biological Engineering and [‡]Department of Applied Physics, Chalmers University of Technology, SE-412 96 Gothenburg, Sweden

Supporting Information

ABSTRACT: Biosensors, in which binding of ligands is detected through changes in the optical or electrochemical properties of a DNA layer confined to the sensor surface, are important tools for investigating DNA interactions. Here, we investigate if conformational changes induced in surface-attached DNA molecules upon ligand binding can be monitored by the quartz crystal microbalance with dissipation (QCM-D) technique. DNA duplexes containing 59−184 base pairs were formed on QCM-D crystals by stepwise assembly of synthetic oligonucleotides of designed base sequences. The DNA films were exposed to the cationic polyamines spermidine and spermine, known to condense DNA molecules in bulk experiments, or to the recombination protein Rad51, known to extend the DNA helix. The binding and dissociation of the ligands to the DNA films were monitored in real time by measurements of the shifts in resonance frequency (Δf) and in dissipation (ΔD). The QCM-D data were analyzed using a Voigt-based model for the viscoelastic properties of polymer films in order to evaluate how the ligands affect thickness and shear viscosity of the DNA layer. Binding of spermine shrinks all DNA layers and increases their viscosity in a reversible fashion, and so does spermidine, but to a smaller extent, in agreement with its lower positive charge. SPR was used to measure the amount of bound polyamines, and when combined with QCM-D, the data indicate that the layer condensation leads to a small release of water from the highly hydrated DNA films. The binding of Rad51 increases the effective layer thickness of a 59bp film, more than expected from the know 50% DNA helix extension. The combined results provide guidelines for a QCM-D biosensor based on ligand-induced structural changes in DNA films. The QCM-D approach provides high discrimination between ligands affecting the thickness and the structural properties of the DNA layer differently. The reversibility of the film deformation allows comparative studies of two or more analytes using the same DNA layer as demonstrated here by spermine and spermidine.

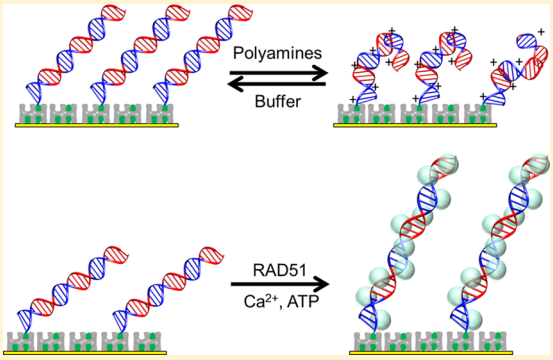

INTRODUCTION

DNA biosensors utilize an oligonucleotide as a recognition element for detecting binding of biomolecules, as used in clinical diagnosis,[1] genetic analysis,[2,3] environmental monitoring,[4] and food analysis.[5] DNA biosensors consisting of single-stranded DNA probes immobilized on a transducer surface may be used to recognize their complementary DNA strands via hybridization,[6,7] but also interactions between DNA and ligands, for instance proteins or small molecules such as duanomycin, may be monitored.[8] So far, DNA biosensors have exploited transducer technologies including electrochemical,[1−3] optical,[9] piezoelectric,[4] and surface plasmon resonance (SPR)[5,10] methods. These methods have demonstrated considerable success regarding rapidness, simplicity, and sensitivity but do not take advantage of information regarding structural changes in the DNA upon binding of the target molecules.

The quartz crystal microbalance with dissipation monitoring (QCM-D) is a powerful tool for real-time detection of biomolecule adsorption to solid/liquid interfaces. It provides simultaneous monitoring of changes in mass and viscoelastic properties of an adsorbed layer through detection of shifts in the resonance frequency (Δf) and the damping (energy dissipation, ΔD) of the oscillatory motion of the quartz sensor. QCM-D has been demonstrated to be a sensitive and efficient tool for the study of recognition reactions, involving DNA,[11−18] proteins,[19−21] lipid membranes,[22−26] and cells.[27−30] Notably, QCM-D measures added mass, including potential hydration—water brought to or removed from the surface by the adsorbing molecule—and changes in water content of the DNA layers can

Received: July 6, 2014
Revised: August 24, 2014
Published: September 8, 2014

ACS Publications © 2014 American Chemical Society

dx.doi.org/10.1021/jp506733w | J. Phys. Chem. B 2014, 118, 11895−11904

be estimated by comparing QCM-D results with corresponding optical measurements by e.g. SPR, from which the added biomolecular mass can be derived. Importantly, QCM-D can provide quantitative data for the effective thickness, shear viscosity, and shear elastic modulus of the layer by using the Voigt-based viscoelastic model[31] to fit Δf and ΔD at multiple harmonics, which has been applied in several QCM-D studies of biomolecules.[11,32,33] QCM-D has proved promising as a biosensing transducer for detecting interactions and conformational changes but has to our knowledge not been used for quantitative studies on how binding of small molecules or proteins to DNA affects its viscoelastic properties. For example, the cationic polyamines spermidine and spermine (+3 and +4, respectively) are two low molecular mass aliphatic amines which are well-known to bind strongly to DNA, resulting in a substantial compaction of the DNA molecules according to bulk solution measurements.[34,35] Rad51 is a key protein in homologous recombination which catalyzes exchange reactions where DNA strands are transferred between two homologous DNA molecules. In the process, Rad51 creates a right-handed helical nucleoprotein filament and thereby stretches the DNA helix by approximately 50% compared to its native B-form length,[36,37] an extension which can be expected to alter the viscoelastic properties of DNA.

We have previously established a DNA platform for QCM-D measurements where a layer of double-stranded DNA (dsDNA) molecules of chosen lengths and sequences were assembled by concatemerization of semicomplementary synthetic oligonucleotides and where the viscoelastic properties of the native DNA film were successfully described by using a frequency-dependent Voigt type of model.[18] In the present study, the polyamine-induced DNA condensation and the extension of the DNA duplex caused by Rad51 filament formation were monitored in real time by QCM-D, complemented by parallel SPR measurements using DNA films assembled in the same manner. The data were analyzed by a viscoelastic model to obtain changes in effective thickness and viscoelastic properties of the DNA film during the binding of the three ligands. The effects on the DNA layer were reversible upon removal of the ligands by rinsing, so the results presented here establish principles for a reusable QCM-D-based DNA biosensor for real-time monitoring of ligand binding through induced conformational changes in the DNA layer.

MATERIALS AND METHODS

Sample Preparation. The buffer used in the formation of DNA films and interaction with Rad51 protein was 1xPBS (10 mM phosphate buffered saline with 27 mM KCl and 137 mM NaCl, at pH 7.4). For DNA−polyamine interactions the buffer was diluted 15 times in water and denoted 0.07xPBS. All samples were prepared using deionized Milli-Q water.

Oligonucleotides were obtained from ATDBio (Southampton, UK); the base sequences and used abbreviations are given in the Supporting Information, Table S1. Each oligonucleotide strand was dissolved in water to a 25 μM stock solution. Oligonucleotides diluted in 1xPBS buffer were used to construct the DNA layers at a concentration of 0.2 μM strands unless otherwise stated.

Stock solutions containing 100 mM spermidine (Sigma-Aldrich, ≥98%) or spermine (Sigma-Aldrich ≥97%) were prepared in water. Human Rad51 was purified as previously described[38] and stored in −80 °C at a concentration of 61 μM in a storage buffer containing 50 mM Tris-HCl at pH 7.6, 1 mM EDTA, 200 mM NaCl, 1 mM dithiothreitol, and 50% glycerol.

Real-Time Interaction Analysis. A QCM-D E4 instrument (Q-sense, Sweden) run at overtones n = 3, 5, 7, 9, and 11 and an SPR BIAcore 2000 system (Biacore, Sweden) were used to monitor DNA film formation and the subsequent binding of polyamines or Rad51 at 22 ± 0.02 °C. AT-cut 5 MHz quartz crystals sputter-coated with a 100 nm thick gold layer onto a 50 nm chromium adhesive layer (Q-Sense, Sweden) for QCM-D measurements, and plain gold-coated chips (SIA kit Au, GE Healthcare, Sweden) for SPR experiments, were biotinylated by forming a mixed self-assembled monolayer following a published protocol.[39] A streptavidin monolayer was formed in situ by adding 25 μg/mL streptavidin (Sigma-Aldrich) in PBS buffer. Solutions of the reagents at indicated constant concentrations were flown over the sensor surfaces of QCM-D and SPR using flow rates of 50 and 10 μL/min, respectively.

DNA Film Formation and DNA−Ligand Interactions. DNA layers with expected lengths (in base pairs) of 59, 85, 159, and 184 bp were constructed on individual QCM-D crystals in 1xPBS buffer. To form 59 bp films, duplexes between b-AB_{59} and $B'A'_{59}$ were prehybridized in 1xPBS and then bound to the streptavidin layer. Longer DNA layers were formed by using a platform for construction of DNA concatemeric layers through stepwise hybridization of single-stranded oligonucleotides in 1xPBS as described elsewhere.[18] The protocol was modified slightly in the present study in order to increase the yield of duplexes. As opposed to performing all the hybridization steps on the surface the b-AB_{59} oligonucleotides were prehybridized with an excess of A'_{34} before immobilizing the formed biotinylated half-duplex to the streptavidin layer. The subsequent sequential hybridization steps followed the reported protocol,[18] including a final step using half-oligonucleotides A or B which ensures fully double-stranded DNA in all the layers and a washing step with 1xPBS buffer after each oligonucleotide addition to remove excess reagent.

Before interacting with the polyamines, the DNA layers were switched to 0.07xPBS by washing the DNA layered surface for 10 min. Thereafter, 5 μM spermidine in 0.07xPBS was introduced to the QCM-D chamber to interact with the DNA film until the binding had reached equilibrium at this constant polyamine concentration. After fully removing the spermidine by changing to 0.07xPBS buffer lacking spermidine, the same DNA layer was exposed to 5 μM spermine in 0.07xPBS. The same procedures for DNA layer formation and polyamine interaction were used in the SPR experiments. In the SPR-based measurements of spermidine and spermine binding isotherms to the DNA layers the polyamine concentration was titrated stepwise from 0.1 to 50 μM. Control QCM-D and SPR experiments with streptavidin layers lacking bound DNA showed that unspecific polyamine binding was negligible (Supporting Information Figure S1).

The DNA binding of Rad51 was studied using a 59 bp DNA layer with reduced coverage of dsDNA strands compared to the spermidine/spermine experiments to mitigate steric constraints when Rad51 forms the bulky nucleoprotein filament in the DNA film. To this end b-AB_{59} was immobilized to the streptavidin layer in two steps by using two additions of a 0.02 μM solution (i.e., 10-fold lower than when forming films for the polyamine experiments), of volumes 600 and 400 μL, respectively, with buffer rinsing in between. Subsequently, the complementary oligonucleotide $B'A'_{59}$ was hybridized to the b-AB_{59} layer. The protein solution used for the Rad51 binding to the 59 bp DNA layer contained 0.2 μM Rad51, 300 μM ATP, 2 mM $CaCl_2$, and 0.2% glycerol in 1xPBS buffer.

Voigt-Based Modeling of the QCM-D Data. The QCM-D data were analyzed using the Voigt-based QTools modeling software (Q-sense, Sweden) for the combined data set of Δf and ΔD at 5 harmonics (n = 3, 5, 7, 9, and 11). The principles of the Voigt-based modeling can be found elsewhere.[31] In the application to DNA films the value of film density and thickness cannot be obtained independently, and we follow the approach of Larsson et al.[11] and assume a fixed value for the density which is consistent with measured values for biomacromolecules in bulk solution. By this approach the Voigt modeling provides values for the effective film thickness, shear viscosity, and shear elastic modulus. The Voigt model used here has frequency-dependent shear viscosity and shear elastic modulus because a previous study[18] demonstrated a substantial improvement in the quality of the fits to concatemeric DNA films.

In the modeling of the experiments with spermidine and spermine the DNA film was treated as a single layer during its formation and the subsequent polyamine interactions. The fluid density and fluid viscosity were set to the values 1000 kg/m^3 and 0.001 kg/ms, respectively, for water at 22 °C, and a fixed value of 1060 kg/m^3 was used for the layer density.[18] Values of the effective thickness, shear viscosity and shear elastic modulus of the DNA layer were then obtained by fitting of the model to the QCM-D data.

For the Rad51 experiments a two-step approach was used to model the DNA-film assembly and protein binding. In the first step the QCM-D data during DNA layer formation was fitted to the Voigt model using the same values for the fluid density and viscosity and the layer density as above. In the second step the effective thickness, shear viscosity and shear elastic modulus parameters for the Rad51−DNA film were fitted using slightly higher fluid density (1020 kg/m^3) and fluid viscosity (0.0012 kg/ms) because the solution in the fluid cell now contained glycerol and a slightly higher layer density (1200 kg/m^3) because the film is a mixture of DNA and proteins.[11]

RESULTS AND DISCUSSION

The aim of the present study was to investigate if the QCM-D technique, in combination with Voigt-based modeling, could be used to characterize ligands binding to DNA, based on changes in DNA layers containing duplexes of four different lengths. We investigated the effects of DNA condensation exerted by two polyamines and the DNA extension caused by Rad51 filament formation. QCM-D was combined with SPR experiments with the aim of evaluating changes in film hydration upon ligand binding. We first present and discuss the results on the interaction between the DNA layer and the two polyamines and thereafter the effects of Rad51 on the DNA layer.

Polyamine-Induced DNA Film Condensation Monitored by QCM-D. *Preparing DNA Films.* DNA layers with chosen lengths of 59, 84, 159, and 184 bp were assembled on four separate QCM-D sensor surfaces in the fluid cell used to expose the formed films to the polyamines. As an example, Figure 1 shows the overall QCM-D signal (at overtone n = 5) upon formation of an 84 bp DNA layer followed by polyamine interaction with this layer. The DNA layer was formed (Figure 1a−c) by first immobilizing a prehybridized duplex between oligonucleotides b-AB$_{59}$ and A′$_{34}$ (see Table S1 for abbreviations and base sequences of all used oligonucleotides). The end of this duplex is designed to expose a 25 base single-strand sequence which is used in the next step ((b) in Figure 1) where the semi-complementary strand A′B′ is hybridized to extend the DNA by 25 bp. Finally the 25 base oligonucleotide A is hybridized to

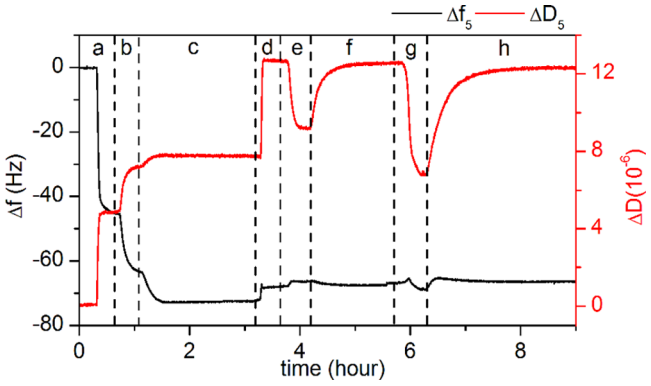

Figure 1. Shifts in frequency Δf (black) and dissipation ΔD (red) (at overtone n = 5) versus time measured by QCM-D during the formation of an 84 bp DNA layer on a preformed streptavidin-modified surface and the subsequent interaction with the polyamines. DNA assembly by subsequent additions of (a) prehybridized b-BA$_{59}$ and A′$_{34}$, (b) A′B′, and (c) A in 1xPBS, followed (d) by a change to 0.07xPBS buffer, (e) addition of spermidine, (f) rinsing with ligand-free 0.07xPBS, (g) addition of spermine, and (h) buffer rinsing.

reach the desired length of 84 bp fully double-stranded DNA. The DNA layers with the other three lengths where formed analogously by changing the number of concatemeric steps, and in all four cases the QCM-D results at five overtones were fitted to a Voigt model (Supporting Information Figure S2) to confirm our previous results on concatemeric DNA layers.[18] The formation of the four types of DNA layers was also investigated by SPR measurements (Supporting Information Figure S3).

Before exposing the DNA layer to the polyamines (Figure 1e−h) the film was transferred to 0.07xPBS buffer because low ionic strength is known to favor DNA condensation by the polyamines in bulk experiments.[34,35] It is seen in Figure 1 (step d) that the decrease in salt concentration compared to the 1xPBS buffer used during the layer assembly increases both Δf and ΔD for the DNA layers. Control experiments (Supporting Information Figure S4) show that these effects are reversible and not associated with loss of DNA from the surface. Figure 1 finally shows the QCM-D responses (at n = 5) during the binding (e) of spermidine to the DNA layer until equilibrium is reached at 5 μM free ligand and the dissociation (f) caused by exposing the condensed layer to 1xPBS buffer. Once all spermidine is removed, the same DNA layer is used to record the corresponding QCM-D responses with spermine (Figure 1g,h). Both polyamines cause a decrease in the dissipation ΔD, whereas Δf increases (less negative) somewhat with spermidine but decreases with spermine at the particular combination of overtone (n = 5) and DNA length (84 bp) presented in Figure 1 (see Figure 2 below for data on the full set of overtones and DNA sizes). Control experiments on streptavidin surfaces without DNA (Supporting Information Figure S1) show that unspecific binding of both polyamines is negligible.

Spermidine. Figure 2a shows typical QCM-D data during the binding and dissociation of spermidine to DNA films containing 59, 84, 159, and 184 bp long DNA molecules. The simultaneously measured changes in frequency and dissipation are displayed as a function of time at five different overtones (n = 3, 5, 7, 9, and 11).

The overall pattern is that the frequency Δf increases (less negative values) for low overtones while a decrease is observed for high overtones, but the details in this pattern depend on the DNA length. For short DNA films (Figure 2a, two top panels)

dx.doi.org/10.1021/jp506733w | J. Phys. Chem. B 2014, 118, 11895−11904

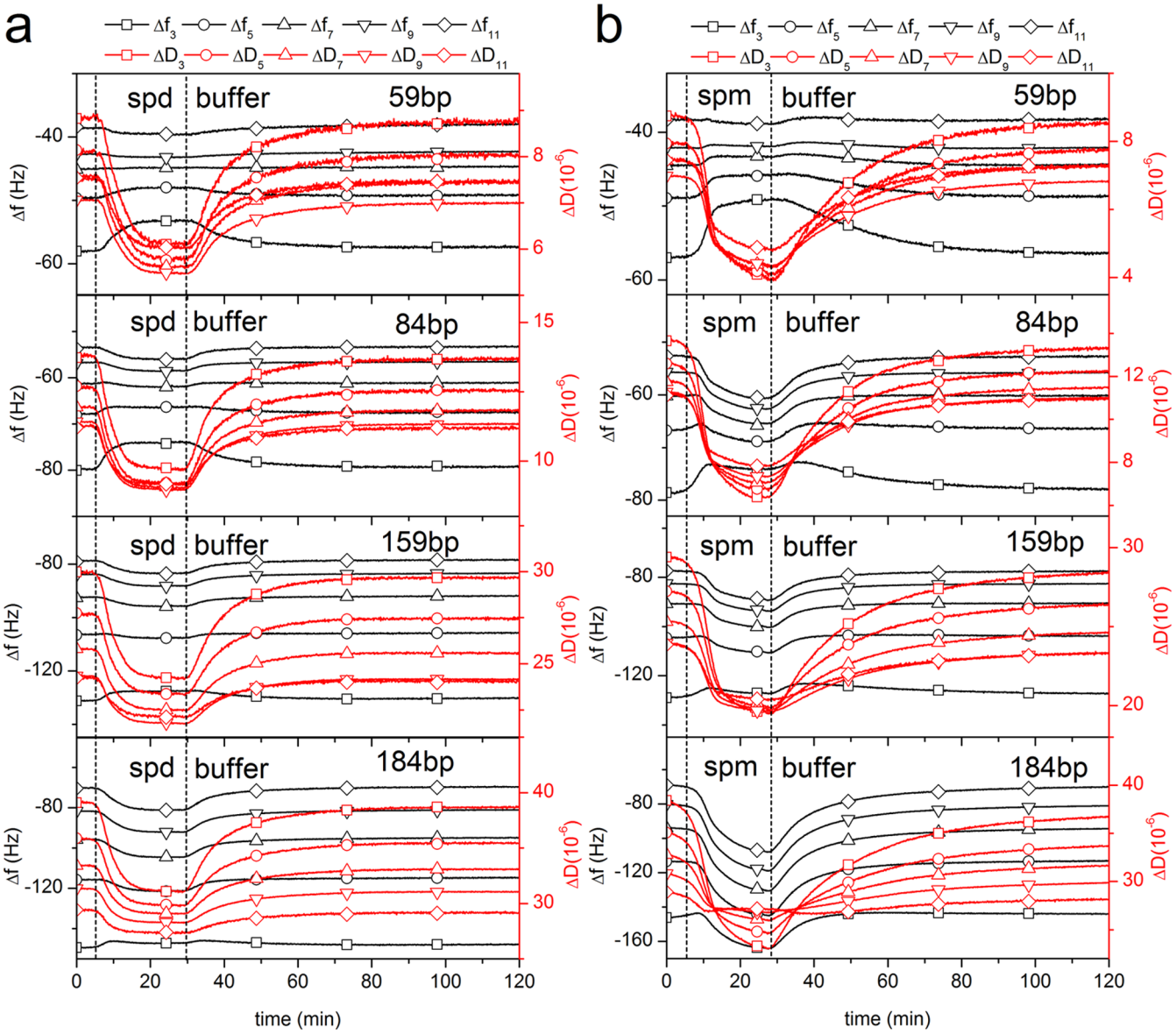

Figure 2. Shifts in frequency Δf (black) and dissipation ΔD (red) (at indicated overtones n = 3, 5, 7, 9, and 11) versus time measured by QCM-D during association and dissociation of (a) 5 μM spermidine (spd) and (b) 5 μM spermine (spm) to DNA layers with assembled lengths of 59, 84, 159, and 184 bp. Buffer used was 0.07xPBS. Spermidine (a) or spermine (b) was added at t = 5 min and ligand-free 0.07xPBS at t = 30 min (dashed lines). Note the different vertical scales.

addition of spermidine leads to an increase in frequency at n = 3 ($\Delta f_{59\ bp}$ = 4.7 Hz and $\Delta f_{84\ bp}$ = 5.9 Hz) and n = 5 ($\Delta f_{59\ bp}$ = 1.5 Hz and $\Delta f_{84\ bp}$ 1.3 Hz), essentially no change at n = 7, and decrease at n = 9 ($\Delta f_{59\ bp}$ = −0.5 Hz and $\Delta f_{84\ bp}$= −1.8 Hz) and n = 11 ($\Delta f_{59\ bp}$ = −1.0 Hz and Δf_{84bp} = −2.6 Hz). For the longer DNA in Figure 2a, the frequency increases only at n = 3 ($\Delta f_{159\ bp}$ = 3.7 Hz and $\Delta f_{184\ bp}$ = 1.9 Hz) and decreases at the higher overtones. By contrast, the dissipation ΔD decreases for all overtones regardless of DNA lengths, indicating that a relatively soft DNA layer becomes stiffer upon binding of spermidine, and the change in dissipation is larger for the longer DNA except at the highest overtones.

Upon rinsing with buffer (at 30 min in Figure 2a) the frequency and dissipation values return to the same level as measured for the nonbound DNA layers before spermidine was added, demonstrating that the binding is reversible. The recovered DNA films were used to study the binding of spermine.

Spermine. Figure 2b shows the QCM-D data upon association and dissociation of 5 μM spermine to the same DNA layers used in the spermidine experiments in Figure 2a. Except for the longest DNA layer (184 bp), spermine exerts similar effects on the DNA layers as spermidine. The frequency increases for low overtones ($\Delta f_{59\ bp}$ = 7.9 Hz, $\Delta f_{84\ bp}$ = 4.5 Hz, and $\Delta f_{159\ bp}$ = 1.9 Hz at overtone n = 3) and decreases for high overtones ($\Delta f_{59\ bp}$ = −0.7 Hz, $\Delta f_{84\ bp}$ = −8.1 Hz, and $\Delta f_{159\ bp}$ = −11.3 Hz at overtone n = 11) in a similar pattern depending on DNA length, and the dissipation decreases at all overtones also when spermine binds. The longest 184 bp DNA layer (Figure 2b bottom panel) shows a different behavior upon interaction with spermine because, in contrast to spermidine, both Δf and ΔD decrease at all overtones. Compared with spermidine, spermine affects the DNA films more strongly because the changes in frequency and dissipation at a given overtone and DNA length are generally more accentuated compared to

dx.doi.org/10.1021/jp506733w | J. Phys. Chem. B 2014, 118, 11895−11904

spermidine. Figure 2 also shows that the dissociation of spermine is slower than for spermidine, suggesting a stronger binding of spermine to the DNA layers.

The changes in frequency and dissipation for different DNA lengths and overtones seen with both polyamines in Figure 2 are related to the viscoelastic properties of the films and the acoustic penetration depth. For instance, the trend from positive to negative changes in Δf with increasing overtone number is typical for soft films which do not obey the Sauerbrey relation for rigid layers.[40] Second, in Figure 2 the dissipation curves at different overtones tend to come closer together when the polyamines are bound compared to the more separated curves for the same DNA layer when naked. Such a weaker sensitivity to overtone number is typical for a more rigid film, which indicates a stiffening/shrinking of the DNA layer in accordance with the overall decrease in ΔD and with the known DNA-condensing effects of spermidine and spermine in bulk experiments. The complex pattern of Δf and ΔD changes is difficult to dissect, however, so these qualitative observations, including the stronger effect of spermine compared to spermidine, were quantified in terms of changes in layer thickness and viscosity by Voigt modeling of the data in Figure 2.

Voigt-Modeled Thickness and Viscoelastic Properties of the Polyamine–DNA Films. The experimental data in Figure 2 were analyzed by fitting to the Voigt-based model (Supporting Information Figure S5), and Figure 3 compares the obtained variations in effective thickness and shear viscosity for the four DNA layers during the binding and dissociation of spermidine and spermine. The modeled shear elastic modulus exhibited a similar variation as the shear viscosity upon the binding of the polyamines (Supporting Information Figure S6).

Figure 3 shows that binding of spermidine and spermine decreases the thickness of the DNA films for all four DNA lengths, while the viscosity increases. These observations clearly show that both polyamines shrink the DNA films and that the condensation makes the DNA layers more rigid. Second, the stronger effect of spermine on both parameters confirms that it condenses the DNA films to a larger extent than spermidine, most probably because the higher positive charge of spermine (4+) than spermidine (3+) leads to a stronger binding to the DNA by electrostatic interactions and thereby causes a more accentuated charge neutralization of the phosphate groups. For the same reason the slower recovery of the spermine-induced shrinkage of the DNA film during the rinsing with polyamine-free buffer in Figure 3 can be explained by an expected slower dissociation of the more strongly bound spermine.

Importantly, the effective layer thickness reflects not only the length of the DNA molecules but also their orientation with respect to the surface. The 59 bp layer in Figure 3a is 12 nm thick before the polyamines are added, considerably thinner than expected for a film of fully perpendicular 59 bp B-form DNA which should be about 20 nm thick (0.34 nm per base pair). Since 59 bp DNA is much shorter than the persistence length of dsDNA (150 bp at the present ionic strength), they can be viewed as rigid rods.[41] The small effective thickness thus implies that they are substantially tilted away from the normal of the surface with a calculated angle of about 37° between the helix axis and the surface, in qualitative agreement with our previous results.[18] Both spermidine and spermine bind in one of the grooves of DNA or externally on the DNA duplex,[42] and as nonintercalators, their binding is not expected to change the contour length of the DNA helix. Thus, the decrease in DNA film thickness likely corresponds to an even more tilted layer,

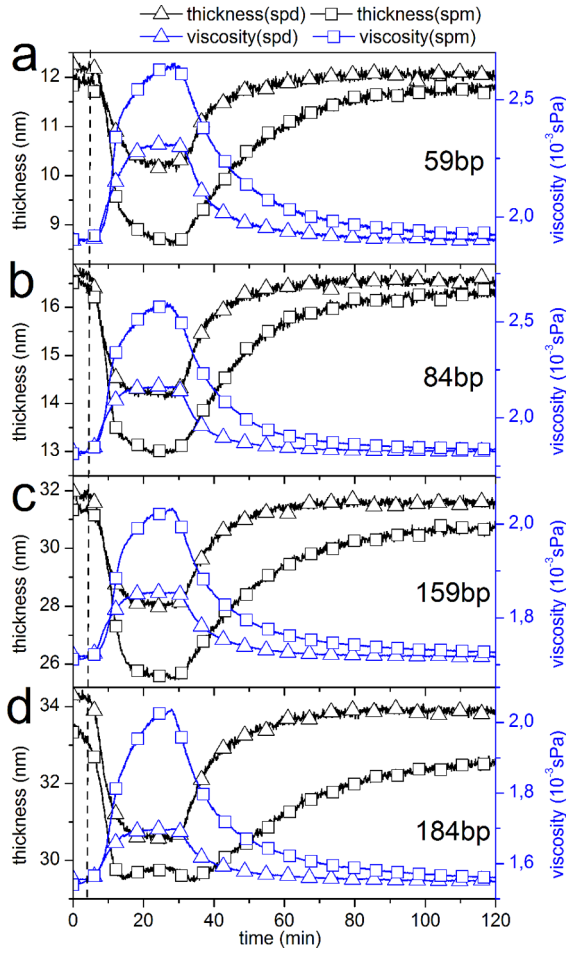

Figure 3. Effect of spermidine (triangles) and spermine (squares) on the effective thickness (black) and shear viscosity (blue) of DNA films with lengths of (a) 59, (b) 84, (c) 159, and (d) 184 bp. The polyamines were added at t = 10 min, polyamine-free 0.07xPBS buffer at t = 30 min. The data are obtained from the fits (Supporting Information Figure S5) of the experimental data in Figure 2 to the Voigt model (see Materials and Methods for details). Note the different vertical scales. Thickness is defined with respect to the streptavidin surface.

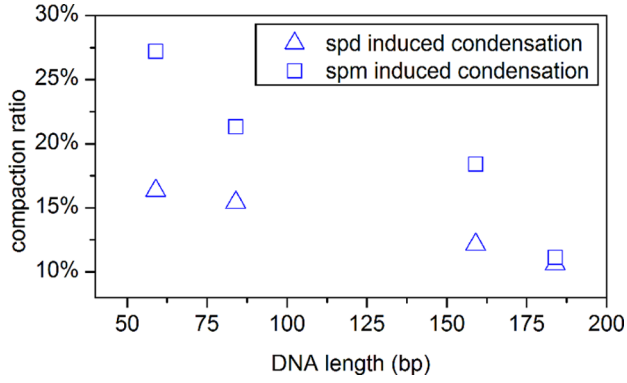

Figure 4. Relative degree of DNA-layer shrinkage by spermidine (triangles) and spermine (rectangles) versus the length of the DNA molecules in the layer. Calculated from the data in Figure 3 on the effective thickness of the nonbound DNA layers and their final polyamine-induced thicknesses.

perhaps assisted by a reduced electrostatic repulsion between the polyamine-bound duplexes due to the added polyamine cationic charges. For spermine the final thickness of 8.8 nm then

dx.doi.org/10.1021/jp506733w | J. Phys. Chem. B 2014, 118, 11895–11904

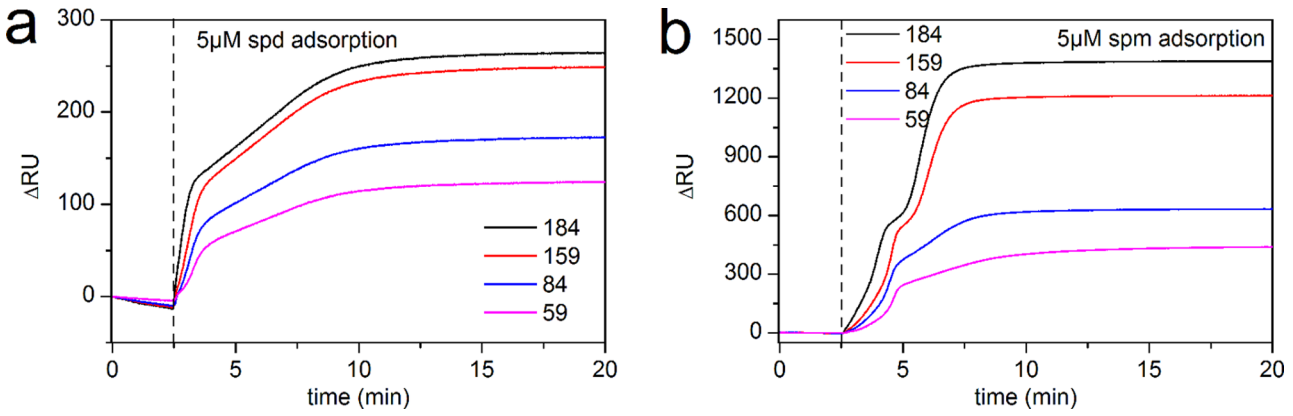

Figure 5. SPR time profiles during the binding of (a) 5 μM spermidine and (b) 5 μM spermine to DNA films with lengths of 59 bp (pink), 84 bp (blue), 159 bp (red), and 184 bp (black) in 0.07xPBS. The polyamines were added at t = 2.5 min.

corresponds to an angle of the helix axis of about 26° to the surface, and for spermidine the corresponding value is 31°.

Figure 4 shows the relative degree of shrinkage compared to the thickness of the original native DNA film, plotted against the DNA length of the four layers. Spermine is almost twice as effective in shrinking the 59 bp layer compared to spermidine. Second, Figure 4 shows that the short DNA layers are compacted to a higher degree by a given polyamine. The weaker relative shrinkage of layers containing longer DNA molecules most likely reflects that they approach, and even surpass the persistence length, and thus tend to coil up on the surface, meaning that they are less extended to start with. Although the effect of spermine or spermidine on the persistence length of DNA is not known to our knowledge, it is expected to be shorter due to the reduced charge density of the duplex. The coil radius will thus decrease and hence also the effective layer thickness, but the polyamine effect may be weakened by the random walk nature of a longer flexible polymer compared to the altered tilt of rod-like short DNA.

Amount of Bound Polyamine and Film Hydration by SPR Measurements. The frequency change in QCM-D reflects the ligand-induced change in acoustically coupled mass, consisting of the bound polyamines and potential changes in the amount of water bound to the DNA films. In fact, the pattern of increase in frequency (less negative values) and decrease in dissipation we observe at low overtones in Figure 2 (most evident when spermine binds to the 59 bp film) was also observed in a study of protein-cross-linking[31] and ascribed to a loss of water during the reaction. We therefore complemented the QCM-D data with SPR measurements to measure the change in biomolecular mass ("dry mass") when the polyamines bind to the DNA films.

Figures 5a and 5b show the SPR responses during the binding of spermidine and spermine, respectively, to the films of the four different DNA lengths under the same conditions as the QCM-D experiments in Figure 2. In both cases, polyamine binding leads to an increase in the biomolecular mass on the surface, where the final values reflect the equilibrium amount of bound ligand at a 5 μM concentration of free ligand in the flowing solution.

Table 1 shows that the equilibrium number of bound polyamines per DNA base pair exhibits no obvious trend with the length of the DNA and that the average values at 5 μM ligand concentration are 1.4 ± 0.2 for spermine and 0.46 ± 0.03 for spermidine. Clearly, spermine binds more strongly than spermidine at the ligand concentration used in Figure 2, which explains the stronger effect on effective thickness and viscosity by spermine seen in Figure 3 as well as the slower layer recovery upon buffer washing.

Table 1. Number of Bound Polyamines per DNA Base Pair[a]

no. of base pairs	spermidine	spermine
59	0.51	1.27
84	0.45	1.19
159	0.45	1.57
184	0.45	1.71
theoretical[b]	0.67	0.50

[a]At equilibrium with 5 μM free polyamine. Calculated from surface-bound masses of polyamines and DNA using Δm_{SPR} values from Table S2 of the Supporting Information and the molecular weights for spermidine (145.3 g/mol), spermine (202.3 g/mol), and the average value per base pair (660 g/mol). [b]Corresponding to charge neutralization of DNA phosphates.

The number of bound spermine molecules per base pair is about 3 times higher than the value of 0.5 needed for charge neutralization of the DNA phosphates, whereas spermidine at 5 μM not quite reaches the corresponding neutralization value of 0.67 for a trivalent ligand. However, measurements of the full binding isotherms by SPR experiments between 0.1 and 50 μM polyamine (Supporting Information Figure S7) show that at binding saturation the DNA films harbor at least 1 spermidine and 1.4 spermine per base pair. The DNA molecules in the films are thus able to bind more than one polyamine charge per phosphate group on the average for both spermidine and spermine.

D'Agostino and co-workers[43] have reported that polyamines at micromolar concentrations can self-assemble with phosphate ions in the millimolar range into supramolecular aggregates. If formed with the phosphate groups in a dense DNA film, such aggregation may help to explain the high number of bound spermine and spermidine per DNA base pair we measure at saturation. The SPR time profiles in Figure 5 indicate that the binding of both spermidine and spermine occurs by two processes. Control experiments in the absence of DNA ruled out unspecific polyamine binding to the streptavidin surface (see Supporting Information S1); thus a possibility is that the biphasic kinetics reflects that the binding to the DNA layers occurs in two sequential steps. Driven by electrostatic interactions, the polyamines are expected to first associate randomly to the DNA molecules. If the high observed binding ratios requires aggregates to form with the phosphate groups in the DNA film, the needed rearrangement of the already bound ligands may be slow in view of that the polyamine dissociation from the films occurs in the order of tens of minutes even when

dx.doi.org/10.1021/jp506733w | J. Phys. Chem. B 2014, 118, 11895−11904

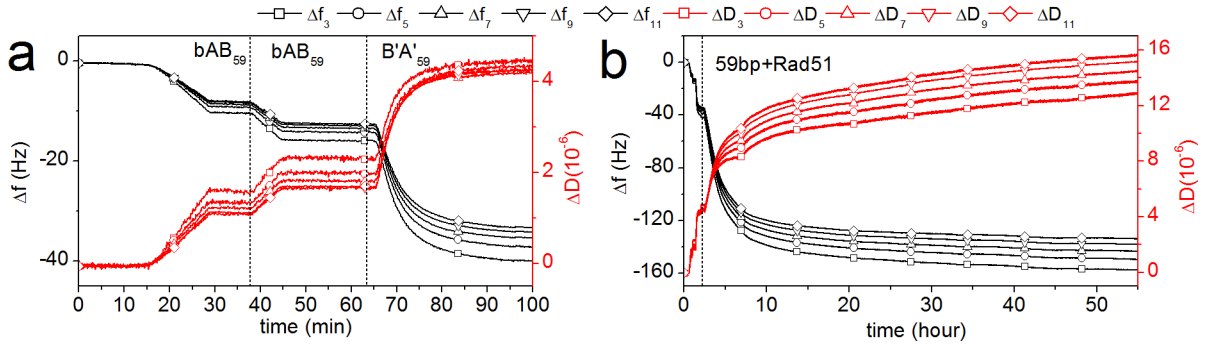

Figure 6. Shifts in frequency (Δf) and dissipation (ΔD) at overtones n = 3 (squares), n = 5 (circle), n = 7 (triangles), n = 9 (inverse triangles), and n = 11 (diamonds) versus time measured by QCM-D during DNA assembly and Rad51 binding. (a) Stepwise formation of a 59bp DNA film with two additions of b-AB_{59} at 15 and 24 min and addition of semicomplementary B′A'_{59} at 62 min. (b) Rad51 association to the same DNA film. Dashed line shows the time of protein addition.

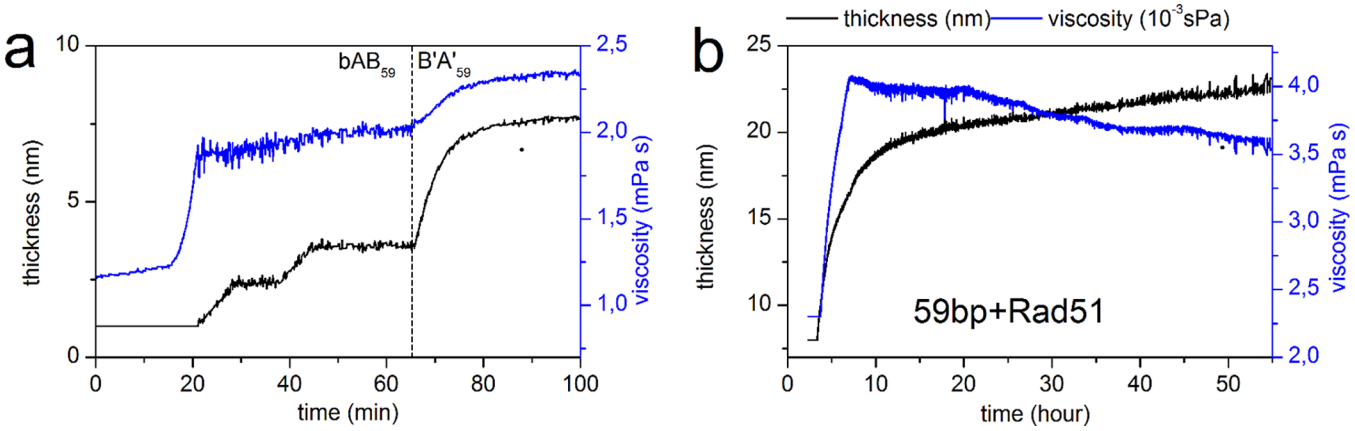

Figure 7. Effective thickness (black) and shear viscosity (blue) versus time during (a) formation of 59 bp DNA film and (b) binding of Rad51 added at t = 4 h. Obtained from the fits (Supporting Information Figure S9) of the data in Figure 6 to the Voigt model (see Materials and Methods for details).

driven by zero free ligand concentration (Figure 3). This is within a time scale comparable to the second step in Figure 5.

Hydration of DNA Films. The observation that the QCM-detected frequency sometimes decreases (Figure 2), even though the dry mass increases under the same conditions (Figure 5), suggests that the polyamine-induced condensation leads to loss of water from the DNA films. The results by QCM-D (acoustic mass or "hydrated mass") and SPR (optical mass or "dry mass") were therefore combined to estimate changes in the degree of DNA film hydration (Supporting Information Table S3). Native DNA films in 0.07xPBS were found to contain 92.0 ± 1.2% water, in agreement with previous studies,[18] and binding of spermidine and spermine reduced this value to 89.8 ± 1.5% and 86.5 ± 2.2%, respectively. The values suggest that only a small amount of water is expelled when the polyamines bind, but more so for spermine, consistent with our observation that it condenses DNA films to a larger extent than spermidine.

Interaction between DNA Films and Rad51 Protein. The results with the two polyamines are consistent with a shrinking due to ligand-induced condensation of the DNA films. In order to investigate if QCM-D also could be used to detect DNA film expansion, we used the protein Rad51, which is known to form a right-handed helical filament around DNA and thereby extending the helix by approximately 50%.[37,44]

Preliminary experiments with the DNA coverage used in the polyamine experiments led to extremely slow Rad51 binding (results not shown). Similarly, Castronovo et al.[45] have observed an impaired binding of restriction enzymes to a high-density DNA film and discussed potential biological implications. In the case of eukaryotic enzymes such as the human Rad51 studied here, DNA crowding effects are probably even more biologically relevant, in view of the high DNA concentration in the nucleus and the large diameter of the Rad51-DNA filament[38] formed during strand exchange in homologous recombination. QCM-D could potentially be used for real-time studies of strand exchange kinetics in a crowded DNA environment of controllable density. As a first step toward this goal, we investigated the effect on the Rad51 binding to a DNA film with reduced coverage (compared to the polyamine experiments above), accomplished by exposing the streptavidin surface to diluted solutions of b-AB_{59} biotinylated DNA (see Materials and Methods).

Figure 6a shows the QCM-D responses at odd overtones 3−11 during the formation of the 59 bp DNA film, where two additions of diluted b-AB_{59} are seen as two stepwise decreases in Δf and increases in ΔD. The final single-stranded b-AB_{59} layer exhibits a frequency and dissipation change (at n = 5) in total by −15 Hz and 2×10^{-6}, respectively, which are lower than the values for the layers used in the polyamine study (−45 Hz and 6×10^{-6} in Figure 1), supporting the assembly of a less dense layer which would provide more space for the Rad51 filaments to form. In the third step in Figure 6a, complementary B′A'_{59} is hybridized to form the 59bp duplex, which approximately doubles the magnitude of the Δf response as expected from the similar size of b-AB_{59} and B′A'_{59}.

dx.doi.org/10.1021/jp506733w | J. Phys. Chem. B 2014, 118, 11895−11904

Figure 6b shows, first, that the binding of Rad51 is very slow compared to the DNA hybridization in Figure 6a, in spite of the reduced DNA coverage, and second that it seems to occur in two steps. The frequency decreases strongly for the first several hours, followed by an even slower decrease that nearly reaches saturation. The dissipation curve also indicates a two-step binding with a faster increase in the beginning, but it approaches saturation more slowly than Δf. Control experiments in the absence of DNA (Supporting Information Figure S8) show that unspecific binding of Rad51 to the streptavidin layer is negligible compared to the changes in frequency and dissipation seen in the presence of DNA. The data in Figure 6 was analyzed by Voigt-based modeling to evaluate how the viscoelastic properties of the DNA film change upon Rad51 interaction.

Modeling of DNA Layer Deformation by Rad51. Figure 7 shows the modeled effective thickness and shear viscosity during the formation of the low coverage DNA film and the binding of Rad51, obtained by Voigt model fitting of the data in Figure 6 (Supporting Information Figure S9).

Starting with the DNA film assembly, Figure 7a shows that the effective thickness increases in two distinct steps due to the two additions of b-AB_{59} and that after hybridization of the complementary $B'A'_{59}$ the final thickness is 7.6 nm. The viscosity of the final double stranded film is 2.3 mPa·s and the shear elastic modulus 0.54 MPa (Supporting Information Figure S10), slightly lower than the starting values for the 59 bp film in Figure 3a (before polyamine addition), which is consistent with the intended lower DNA coverage in the films for the Rad51 experiments. That the final thickness is lower than the 12 nm for the denser 59 bp films in Figure 3a indicates that the rod-like DNA molecules tilt even more in the less dense films, with an angle of about 22° to the surface instead of the value 37°, deduced above (Figure 3a).

Figure 7b shows the modeled effective thickness and shear viscosity during the binding of Rad51 to the low coverage DNA film. The thickness increases monotonically to 22 nm upon Rad51 binding, seemingly in two steps as is clearly supported by the nonmonotonic behavior in shear viscosity and shear modulus (Supporting Information Figure S10) which both exhibits a maximum at about $t = 7$ h. Viscosity shows a rapid increase to 4 mPa·s and then decreases slowly, reaching 3.6 mPa·s after 50 h. Similarly, the shear modulus shows a fast increase to 0.7 MPa initially followed by a slow decline to 0.5 MPa.

The increase in viscosity and shear modulus is consistent with formation of Rad51−DNA filaments, which are known to be more rigid than double-stranded DNA.[46,47] The increase in layer thickness from 7.6 to 22 nm, on the other hand, is considerably larger than expected from bulk experiments,[44,48] which report only a 50% increase in DNA length by Rad51. Again it should be remembered that the change in effective layer thickness will reflect not only the lengthening of the DNA helix by Rad51 but also potential changes in the orientation of the DNA rods relative to the surface. One possibility is that the tilted DNA molecules may be forced to become closer to perpendicular to the surface because the Rad51−DNA filament takes up more space on the surface than the duplex itself due to its significantly larger diameter. If the 59 bp DNA was fully covered with Rad51, and stood perpendicular to the surface, the expected film thickness would be 30 nm. The value 22.5 nm after 50 h in Figure 7b is lower, but the thickness clearly continues to increase, which suggests that the Rad51−DNA film approaches this hypothetical value at equilibrium.

A simple model for the two-phase binding in Figure 7b is that the first step (up to the maximum in the viscosity) corresponds to Rad51 binding and extending the tilted DNA duplexes making them more rigid, followed by a slow rearrangement where the bulky nucleoprotein filaments approach a perpendicular orientation. However, the effective thickness of about 18 nm at the viscosity maximum is larger than the 11 nm value expected for a film of fully extended filaments with an angle of 22° to the surface, so even the first step most likely involves a reduced tilting of the DNA molecules. In the second step, the viscosity and shear modulus decrease, while the layer thickness increases slowly, indicating a softening of the layer perhaps by a slow arrangement of the Rad51 molecules among the DNA molecules. Understanding this complex binding process requires further studies, but at any rate, we note that the Rad51 binding to DNA can be monitored through a monotonous increase in the effective film thickness.

■ CONCLUDING REMARKS

The principles of a QCM-D based biosensor for detecting conformational changes in DNA films was demonstrated through investigations of interactions with two polyamines and the Rad51 protein. The DNA deformation induced by spermidine and spermine can be directly detected by QCM-D whereas the same processes monitored by SPR provide the bound biomolecular mass. The approach lends credibility from the observation that spermine consistently affects the DNA layer more than spermidine regarding the dissipation changes (Figure 2), modeled layer thickness and viscosity (Figure 3) and degree of hydration, in agreement with the higher amount of bound spermine measured independently by SPR (Figure 5). The extension of DNA molecules in a film caused by filament formation of Rad51 protein is also clearly detectable by QCM-D.

The complex effect of overtone and DNA length in the film makes direct interpretation of the QCM-D responses (Figure 2) difficult. The observation that the frequency decreases for the higher overtones with both spermine and spermidine is seemingly contradictory since SPR shows a binding of the polyamines. Expulsion of water upon the condensation is a part of the answer since QCM-D measures acoustically coupled mass including water, but the decrease in hydration is rather modest (a few percentage points) so the condensed DNA films remain highly hydrated. A second and probably larger contribution can be understood from our previous experimental and theoretical studies of the QCM-D response of DNA films up to several hundred base pairs thick.[18] For such DNA layers, the changes in frequency and dissipation show reversed signs at a certain layer thickness even though longer DNA concatemers are formed at the surface. By Voigt modeling the complex changes in frequency and dissipation at different overtones in QCM-D experiments can be converted into the effective physical properties thickness, viscosity, and shear modulus of the film. The modeling results show that polyamine-induced DNA condensation results in a reduction of the effective DNA film thickness, whereas Rad51 binding to DNA instead causes a strong increase of the layer thickness. Importantly, molecular interpretation of the effective thickness requires that both the length of the DNA−ligand complexes and their orientation relative to the surface are taken into account as well as water content.

From a DNA biosensor point of view, the modeled layer thickness is the most discriminatory output: the polyamines and Rad51 induce opposite effects on the effective thickness, whereas both increase the modeled layer viscosity. Second, the

fact that the native DNA film can be regenerated allows comparative studies (as spermidine and spermine illustrate here), which can be useful when comparing the effects of an unknown analyte with a known reference substance. Third, the Rad51 experiments show that the coverage of target DNA molecules on the surface may have to be tailored to the analyte under investigation. A less dense layer is helpful if the analyte is bulky and the impractically slow response of Rad51 could probably be sped up further by an even lower DNA coverage. Fourth, a film of short DNA molecules is preferable because in thick DNA films the response to added mass is not linear or even monotonous[18] due to effects of the penetration depth, so a ligand-induced change in the film thickness may in itself alter how the QCM-D detected Δf depends on the added mass. Finally, our concatemeric approach allows the base sequence of the investigated DNA to be designed at will, which may be important in studies of ligand binding, since it is often sensitive to the DNA sequence.

■ ASSOCIATED CONTENT

Supporting Information

Base sequences of oligonucleotides (Table S1), QCM-D and SPR measurement of unspecific binding of polymines on SA layer (Figure S1), QCM-D measurement and Voigt-based modeling of DNA film formation (Figure S2), SPR measurements of DNA film formation (Figure S3), QCM-D measurements during buffer switching (Figure S4), Voigt-based modeling of DNA−polyamine interaction (Figure S5), changes in shear elastic modulus upon polyamine condensation of DNA films (Figure S6), summary of masses of DNA films from QCM-D and SPR (Table S2), estimates of DNA film hydration (Table S3), polyamine binding isotherms from SPR experiments (Figure S7), control experiment for unspecific binding of Rad51 to streptavidin layer (Figure S8), Voigt-based modeling of DNA−Rad51 interaction (Figure S9), and changes in shear elastic modulus upon Rad51 to DNA films (Figure S10). This material is available free of charge via the Internet at http://pubs.acs.org.

■ AUTHOR INFORMATION

Corresponding Author

*E-mail baa@chalmers.se (B.Å.).

Notes

The authors declare no competing financial interest.

■ ACKNOWLEDGMENTS

This work was supported by the Area of advance in Nanoscience and Nanotechnology at Chalmers University of Technology and King Abdullah University of Science and Technology Grant [KUK-11-008-23 to L.F.]. B.Å., S.S., and F.W. acknowledge financial support from the Swedish Research Council.

■ REFERENCES

(1) Wang, J.; Ozsoz, M.; Cai, X.; Rivas, G.; Shiraishi, H.; Grant, D. H.; Chicharro, M.; Fernandes, J.; Palecek, E. Interactions of antitumor drug daunomycin with DNA in solution and at the surface. *Bioelectrochem. Bioenerg.* **1998**, *45* (1), 33−40.

(2) Ding, C.; Zhao, F.; Zhang, M.; Zhang, S. Hybridization biosensor using 2,9-dimethyl-1,10-phenantroline cobalt as electrochemical indicator for detection of hepatitis B virus DNA. *Bioelectrochemistry* **2008**, *72* (1), 28−33.

(3) Wang, K.; Chen, J.; Chen, J.; Liu, A.; Li, G.; Luo, H.; Lin, X.; Chen, Y. A sandwich-type electrochemical biosensor for detection of BCR/ABL fusion gene using locked nucleic acids on gold electrode. *Electroanalysis* **2009**, *21* (10), 1159−1166.

(4) Mo, X.-T.; Zhou, Y.-P.; Lei, H.; Deng, L. Microbalance-DNA probe method for the detection of specific bacteria in water. *Enzyme Microb. Technol.* **2002**, *30* (5), 583−589.

(5) Feriotto, G.; Borgatti, M.; Mischiati, C.; Bianchi, N.; Gambari, R. Biosensor technology and surface plasmon resonance for real-time detection of genetically modified roundup ready soybean gene sequences. *J. Agric. Food Chem.* **2002**, *50* (5), 955−962.

(6) Sassolas, A.; Leca-Bouvier, B. D.; Blum, L. J. DNA biosensors and microarrays. *Chem. Rev.* **2008**, *108* (1), 109−139.

(7) Teles, F. R. R.; Fonseca, L. P. Trends in DNA biosensors. *Talanta* **2008**, *77* (2), 606−623.

(8) Tombelli, S.; Palchetti, I.; Mascini, M. Nucleic acids-based biosensors. In *Materials Science of DNA*; CRC Press: Boca Raton, FL, 2012; pp 291−309.

(9) Piunno, P. A. E.; Krull, U. J.; Hudson, R. H. E.; Damha, M. J.; Cohen, H. Fiber optic biosensor for fluorometric detection of DNA hybridization. *Anal. Chim. Acta* **1994**, *288* (3), 205−14.

(10) Yang, N.; Su, X.; Tjong, V.; Knoll, W. Evaluation of two- and three-dimensional streptavidin binding platforms for surface plasmon resonance spectroscopy studies of DNA hybridization and protein-DNA binding. *Biosens. Bioelectron.* **2007**, *22* (11), 2700−2706.

(11) Larsson, C.; Rodahl, M.; Höök, F. Characterization of DNA immobilization and subsequent hybridization on a 2D arrangement of streptavidin on a biotin-modified lipid bilayer supported on SiO_2. *Anal. Chem.* **2003**, *75*, 5080−5087.

(12) Tang, W.; Wang, D.; Xu, Y.; Li, N.; Liu, F. A self-assembled DNA nanostructure-amplified quartz crystal microbalance with dissipation biosensing platform for nucleic acids. *Chem. Commun.* **2012**, *48* (53), 6678−6680.

(13) Nguyen, T. H.; Elimelech, M. Adsorption of plasmid DNA to a natural organic matter-coated silica surface: Kinetics, conformation, and reversibility. *Langmuir* **2007**, *23*, 3273−3279.

(14) Nguyen, T. H.; Chen, K. L. Role of divalent cations in plasmid DNA adsorption to natural organic matter-coated silica surface. *Environ. Sci. Technol.* **2007**, *41*, 5370−5375.

(15) Nguyen, T. H.; Elimelech, M. Plasmid DNA adsorption on silica: Kinetics and conformational changes in monovalent and divalent salts. *Biomacromolecules* **2007**, *8*, 24−32.

(16) Rawle, R. J.; Selassie, C. R. D.; Johal, M. S. Creation of mammalian single- and double-stranded DNA surfaces: A real-time QCM-D study. *Langmuir* **2007**, *23*, 9563−9566.

(17) Woller, J. G.; Börjesson, K.; Svedhem, S.; Albinsson, B. Reversible hybridization of DNA anchored to a lipid membrane via porphyrin. *Langmuir* **2012**, *28* (4), 1944−1953.

(18) Sun, L.; Svedhem, S.; Åkerman, B. Construction and modelling of concatemeric DNA multilayers on a planar surface as monitored by QCM-D and SPR. *Langmuir* **2014**, *30* (28), 8432−8441.

(19) Minunni, M.; Mascini, M.; Guilbault, G. G.; Hock, B. The quartz crystal microbalance as biosensor. A status report on its future. *Anal. Lett.* **1995**, *28*, 749−64.

(20) Welle, A.; Chiumiento, A.; Barbucci, R. Competitive protein adsorption on micro patterned polymeric biomaterials, and viscoelastic properties of tailor made extracellular matrices. *Biomol. Eng.* **2007**, *24*, 87−91.

(21) Bluemmel, J.; Perschmann, N.; Aydin, D.; Drinjakovic, J.; Surrey, T.; Lopez-Garcia, M.; Kessler, H.; Spatz, J. P. Protein repellent properties of covalently attached PEG coatings on nanostructured SiO_2-based interfaces. *Biomaterials* **2007**, *28*, 4739−4747.

(22) Kunze, A.; Zhao, F.; Marel, A.-K.; Svedhem, S.; Kasemo, B. Ion-mediated changes of supported lipid bilayers and their coupling to the substrate. A case of bilayer slip? *Soft Matter* **2011**, *7* (18), 8582−8591.

(23) Keller, C. A.; Kasemo, B. Surface specific kinetics of lipid vesicle adsorption measured with a quartz crystal microbalance. *Biophys. J.* **1998**, *75*, 1397−1402.

(24) Reimhult, E.; Zaech, M.; Höök, F.; Kasemo, B. A multitechnique study of liposome adsorption on Au and lipid bilayer formation on SiO_2. *Langmuir* **2006**, *22*, 3313−3319.

(25) Edvardsson, M.; Svedhem, S.; Wang, G.; Richter, R.; Rodahl, M.; Kasemo, B. QCM-D and reflectometry instrument: Applications to supported lipid structures and their biomolecular interactions. *Anal. Chem.* **2009**, *81*, 349−361.
(26) Richter, R. P.; Berat, R.; Brisson, A. R. Formation of solid-supported lipid bilayers: An integrated view. *Langmuir* **2006**, *22* (8), 3497−3505.
(27) Tymchenko, N.; Kunze, A.; Dahlenborg, K.; Svedhem, S.; Steel, D. Acoustical sensing of cardiomyocyte cluster beating. *Biochem. Biophys. Res. Commun.* **2013**, *435* (4), 520−525.
(28) Schofield, A. L.; Rudd, T. R.; Martin, D. S.; Fernig, D. G.; Edwards, C. Real-time monitoring of the development and stability of biofilms of Streptococcus mutans using the quartz crystal microbalance with dissipation monitoring. *Biosens. Bioelectron.* **2007**, *23*, 407−413.
(29) Thorslund, S.; Larsson, R.; Nikolajeff, F.; Bergquist, J.; Sanchez, J. Bioactivated PDMS microchannel evaluated as sensor for human CD4+ cells-The concept of a point-of-care method for HIV monitoring. *Sens. Actuators, B* **2007**, *B123*, 847−855.
(30) Saitakis, M.; Gizeli, E. Acoustic sensors as a biophysical tool for probing cell attachment and cell/surface interactions. *Cell. Mol. Life Sci.* **2012**, *69* (3), 357−371.
(31) Voinova, M. V.; Rodahl, M.; Jonson, M.; Kasemo, B. Viscoelastic acoustic response of layered polymer films at fluid-solid interfaces: continuum mechanics approach. *Phys. Scr.* **1999**, *59* (5), 391−396.
(32) Höök, F.; Kasemo, B.; Nylander, T.; Fant, C.; Sott, K.; Elwing, H. Variations in coupled water, viscoelastic properties, and film thickness of a Mefp-1 protein film during adsorption and cross-linking: A quartz crystal microbalance with dissipation monitoring, ellipsometry, and surface plasmon resonance study. *Anal. Chem.* **2001**, *73* (24), 5796−5804.
(33) Graneli, A.; Edvardsson, M.; Höök, F. DNA-based formation of a supported, three-dimensional lipid vesicle matrix probed by QCM-D and SPR. *ChemPhysChem* **2004**, *5*, 729−733.
(34) Gosule, L. C.; Schellman, J. A. DNA condensation with polyamines. I. Spectroscopic studies. *J. Mol. Biol.* **1978**, *121* (3), 311−26.
(35) Chattoraj, D. K.; Gosule, L. C.; Schellman, J. A. DNA condensation with polyamines. II. Electron microscopic studies. *J. Mol. Biol.* **1978**, *121* (3), 327−37.
(36) Stasiak, A.; Di Capua, E.; Koller, T. Elongation of duplex DNA by recA protein. *J. Mol. Biol.* **1981**, *151* (3), 557−64.
(37) Benson, F. E.; Stasiak, A.; West, S. C. Purification and characterization of the human Rad51 protein, an analogue of E. coli RecA. *EMBO J.* **1994**, *13* (23), 5764−71.
(38) Reymer, A.; Frykholm, K.; Morimatsu, K.; Takahashi, M.; Norden, B. Structure of human Rad51 protein filament from molecular modeling and site-specific linear dichroism spectroscopy. *Proc. Natl. Acad. Sci. U. S. A.* **2009**, *106* (32), 13248−13253.
(39) Nilebäck, E.; Feuz, L.; Uddenberg, H.; Valiokas, R.; Svedhem, S. Characterization and application of a surface modification designed for QCM-D studies of biotinylated biomolecules. *Biosens. Bioelectron.* **2011**, *28* (1), 407−413.
(40) Hook, F.; Rodahl, M.; Brzezinski, P.; Kasemo, B. Energy dissipation kinetics for protein and antibody-antigen adsorption under shear oscillation on a quartz crystal microbalance. *Langmuir* **1998**, *14* (4), 729−734.
(41) Sobel, E. S.; Harpst, J. A. Effects of Na^+ on the persistence length and excluded volume of T7-bacteriophage DNA. *Biopolymers* **1991**, *31* (13), 1559−1564.
(42) Liquori, A. M.; Costanti, L.; Crescenz, V.; Elia, V.; Giglio, E.; Puliti, R.; Desantis, M.; Vitaglia, V. Complexes between DNA and polyamines - A Molecular model. *J. Mol. Biol.* **1967**, *24* (1), 113.
(43) Di Luccia, A.; Picariello, G.; Iacomino, G.; Formisano, A.; Paduano, L.; D'Agostino, L. The in vitro nuclear aggregates of polyamines. *FEBS J.* **2009**, *276* (8), 2324−2335.
(44) Ogawa, T.; Yu, X.; Shinohara, A.; Egelman, E. H. Similarity of the yeast RAD51 filament to the bacterial RecA filament. *Science* **1993**, *259* (5103), 1896−9.
(45) Castronovo, M.; Lucesoli, A.; Parisse, P.; Kurnikova, A.; Malhotra, A.; Grassi, M.; Grassi, G.; Scaggiante, B.; Casalis, L.; Scoles, G. Two-dimensional enzyme diffusion in laterally confined DNA monolayers. *Nat. Commun.* **2011**, *2* (May), 1296/1−1296/10.
(46) van der Heijden, T.; Seidel, R.; Modesti, M.; Kanaar, R.; Wyman, C.; Dekker, C. Real-time assembly and disassembly of human RAD51 filaments on individual DNA molecules. *Nucleic Acids Res.* **2007**, *35* (17), 5646−5657.
(47) Fornander, L. H.; Frykholm, K.; Reymer, A.; Renodon-Corniere, A.; Takahashi, M.; Norden, B. Ca^{2+} improves organization of single-stranded DNA bases in human Rad51 filament, explaining stimulatory effect on gene recombination. *Nucleic Acids Res.* **2012**, *40* (11), 4904−4913.
(48) Conway, A. B.; Lynch, T. W.; Zhang, Y.; Fortin, G. S.; Fung, C. W.; Symington, L. S.; Rice, P. A. Crystal structure of a Rad51 filament. *Nat. Struct. Mol. Biol.* **2004**, *11* (8), 791−796.